A RAPID 3-D PASSIVE VORTEX MICROMIXER UTILIZING SELF-ROTATION EFFECT

Lung-Ming Fu[1], Chia-Yen Lee[**], Che-Hsin Lin[***], Chien-Hsiung Tsai[****], and Guan-Liang Chang[*****]

[*]Graduate Institute of Materials Engineering
National Pingtung University of Science and Technology, Pingtung, Taiwan
[**]Department of Mechanical and Automation Engineering, Da-Yeh University, Taiwan
[***]Department of Mechanical and Electro-mechanical Engineering,
National Sun Yat-sen University, Kaohsiung, Taiwan
[****]Department of Vehicle Engineering,
National Pingtung University of Science and Technology, Pingtung, Taiwan
[*****]Institute of Biomedical Engineering, National Cheng-Kung University, Tainan, Taiwan

loudyfu@mail.npust.edu.tw, cy@mail.dyu.edu.tw and chehsin@mail.nsysu.edu.tw

Abstract: This paper proposes a novel 3-dimensional (*3-D*) vortex micromixer for micro-total analysis systems (μTAS) applications which utilizes self-rotation effects to mix fluids in a circular chamber at low Reynolds numbers (*Re*). The microfluidic mixer is fabricated in a three-layer glass structure for delivering fluid sample in parallel. The fluids are driven into the circular mixing chamber by means of hydrodynamic pumps from two fluid inlet ports. The two inlet channels divide into 8 individual channels tangent to a 3-D circular chamber for mixing purpose. Numerical simulation of the microfluidic dynamics is employed to predict the self-rotation phenomenon and to estimate the mixing performance under various Reynolds number conditions. Experimental flow visualization by mixing dye samples is performed in order to verify the numerical simulation results. A good agreement is found to exist between the two sets of results. The numerical results indicate that the mixing performance can be as high as 90% within a mixing chamber of 1 mm diameter when the Reynolds number is Re = 4. Additionally, the results confirm that self-rotation in the circular mixer enhances the mixing performance significantly, even at low Reynolds numbers. The novel micromixing method presented in this study provides a simple solution to mixing problems in the Lab-chip system.

Introduction

Micro-total-analysis-system research aimed at developing miniaturized and integrated "Lab-on-a-chip" devices for biochemical analysis applications has made significant progress in recent years [1]. Miniaturization has many fundamental advantages, including: (1) a higher throughput (achieved by way of parallelization), (2) reduced sample consumption volumes, (3) shorter analysis times, (4) the feasibility of in-situ operation, (5) improved performance and reliability, and (6) reduced operating and manufacturing costs.[6] A typical micro-total-analysis-system device includes a number of functional units such as sample mixers, reactors, injectors, separators, collectors, filters, sorters, pre-concentrators, cytometers, and on-line detection arrangements [2]. In a concept commonly referred to as "Lab-on-a-chip", several of these components are integrated serially on a microchip in order to carry out a complete assay of a material [3].

Micromixers are commonly employed in chemical or biological analyses. The mixing performance is a fundamentally important aspect of these devices since it is this mixing which generates the biochemical reactions necessary for their successful operation. However, it is difficult to mix fluids in microfluidic systems since the low Reynolds number of typical flows in microfluidic devices results in the formation of laminar flow. Furthermore, the characteristic size of the microchannels incorporated in these devices is too small to generate disordered flows. A review of the related literature reveals that various micromixers have been designed and developed. These devices may broadly be categorized as being either active or passive in nature. Active micromixers generally enhance mixing by stirring the flow in order to create secondary flows. This stirring effect can either be achieved mechanically [4] or by means of magneto-hydrodynamic [5], instable hydroelectrokinetic pumping [6], pressure perturbation [8], micro-jet arrays [9], or acoustic streaming [10] techniques. The secondary flows stretch and fold the material lines, thereby reducing the diffusion path between the fluid streams, and hence enhancing the mixing effect. Active microfluidic mixers are particularly suitable for chamber mixing. However, fabricating this type of microfluidic mixer is rather complex. Furthermore, these devices generally require some form

ISSN: 1727-1983

of external power sources and control systems.

Many passive microfluidic mixers have been developed in recent years. Bessoth *et al* [11] presented a passive mixer which reduced the diffusion path between the fluid streams by first splitting and then recombining the flow. Liu *et al.* [12] fabricated passive chaotic microfluidic mixers incorporating 3-dimensional serpentine microchannels. The flow in the 3-dimensional serpentine channels demonstrated chaotic advection at high flow rates (i.e. at Reynolds numbers of approximately 70) and provided an effective mixing performance. Johnson *et al.* [13] presented a T-shaped micromixer which utilized a series of slanted wells at the junction to promote the rapid mixing of two confluent streams undergoing electroosmotic flow. However, a high-power micro-pump was required to stir the flow sample sufficiently to generate chaotic mixing. The use of patterned grooves to achieve mixing in microchannels has been studied both experimentally and numerically. The results have indicated that the associated fluid stream rotation and chaotic advection effects successfully enhance the mixing performance. [14] Burke *et al.* [15] presented stopped-flow enzyme assays using microfabricated static mixers and demonstrated that these devices delivered a similar performance to that obtained using an external mixing device. For example, Chung *et al.* [16] proposed a passive micromixer utilizing self-circulation of the fluid in the mixing chamber. The numerical results indicated that this type of micromixer was capable of delivering an enhanced mixing performance, particularly at Reynolds numbers in the range of 20 to 400. Kim *et al.* [17] used 3-dimensional barrier embedded micromixers to enhance the mixing performance in a microchannel at low Reynolds numbers (i.e. approximately 28). Various alternative forms of passive microfluidic mixing techniques have been investigated and developed.

Typically, passive micromixers first introduce the sample fluids to be mixed into the mixing device through two inlet channels and then mix these fluids in a third channel. Therefore, when two or more sample fluids are injected into the same channel (or chamber) simultaneously, the resulting mixing efficiency will be far higher since diffusive effects cause the contact area of the various samples to be increased. The present study develops a novel passive micromixer which utilizes self-rotation of the sample fluids from multiple injection channels to produce 3-dimensional vortexes in the circular mixing chamber at low Reynolds numbers, thereby enhancing the mixing performance. Figure 1 presents a schematic illustration of the proposed vortex micromixer device. The fluids to be mixed enter the circular chamber at a low Reynolds number through the eight tangential inlets. The simple fabrication process and low driving force of this mixing method make the proposed micromixer is suitable for low-cost analytical applications.

Experiment section

In order to ensure a stable flow during the experimental tests, the fluid channels in the proposed micromixing device are designed to be of equal length such that the flow resistance within each channel is equal. A multilayer microfluidic chip is required to achieve channel crossovers for the different fluid samples. In this regards, three layers of glass substrate to fabricate the microfluidic device in a sandwich structure. Furthermore, the proposed device is driven by syringe pumps and hence a high pressure is capable of being generated in the microchannels during operation. Therefore, the microchip must have high mechanical and bonding strengths if it is to withstand the high internal pressure. Hence, the present study deliberately adopts the use of low-cost soda-lime glass substrates to fabricate the microchip devices rather than the more conventional choice of plastic or silicon based substrates [18]. Figure 2 presents a simplified schematic representation of the fabrication process used in the present study. Initially, the microscope slides were cleaned in a boiling piranha solution. (Piranha solutions are extremely energetic and may result in explosion or skin burns if not handled with extreme caution.) The lower substrate was then patterned with positive photoresist (AZ 4620, Clariant Corp., USA) in a conventional photolithography procedure (Fig. 2(a)). The patterned glass substrate was then immersed in a BOE (buffered oxide etch, J T Baker, USA) bath for 40 min to generate the required microchannels (Fig 2(b)).

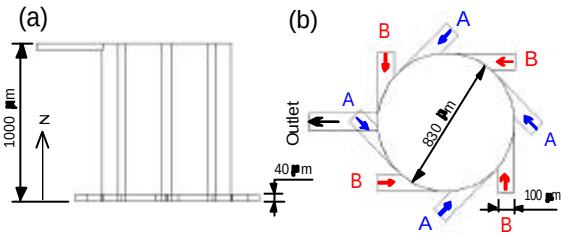

Figure 1: Schematic illustration of circular microchamber mixer geometry: (a) side view and (b) top view.

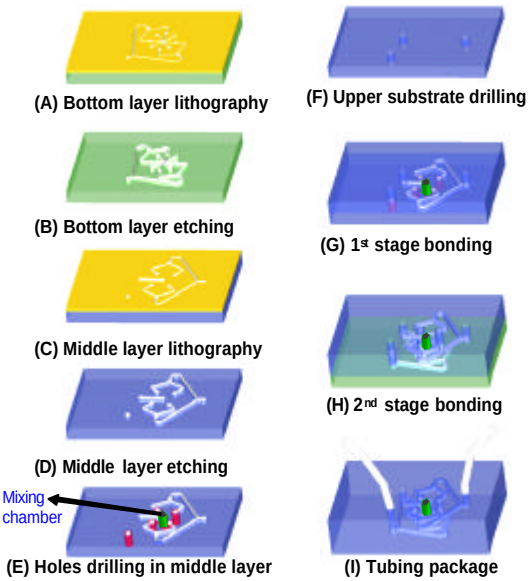

Figure 2: Simplified schematic representation of fabrication process employed for proposed micromixer.

ISSN: 1727-1983

After etching for 40 min with ultrasonic agitation, the microchannel attained a depth of 36 µm. The middle glass substrate in the sandwich structure was fabricated using the same lithography and etching procedures as discussed above (Figs. 2(c) and 2(d)). Fluid-via-holes and the mixing chamber were then drilled into the etched middle layer using a diamond drill-bit (Fig. 2(e)). Meanwhile, a bare glass substrate, designed to act as the upper layer to seal the microchannels, was drilled with via holes to form the sample inlet holes (Fig 2(f)). After preparing the individual glass substrates, each substrate was cleaned once again in a boiling piranha solution prior to the bonding process. A high yield two-stage fusion bonding process was used to guarantee a high-strength bonding result. In the first stage, the upper and middle glass substrates were bonded in a 580°C sintering oven for 20 min (Fig. 2(g)). In the second stage, the process was repeated to bond the bottom substrate to the previously sealed substrate (Fig. 2(h)). Finally, Teflon tubing with a 1.5 mm outer diameter and a 500 µm inner diameter was attached to each inlet hole. These tubes served to connect the microchip device to the actuating syringes used to drive the individual fluid samples.

Fig. 3(a) presents a photographic image of the assembled cyclic mixer. The fabricated chip measures 26 mm in width and 40 mm in length and has a mixing chamber 830 µm in diameter and 1 mm in height. It can be seen that a sample outlet channel with a width of 100 µm and a depth of 40 µm is located perpendicularly to the mixing channel between the upper and middle substrates. Note that the geometries and lengths of the sample channels leading from the sample inlet to the mixing chamber are equal to ensure that the flow resistances in the various channels are also equal. Fig. 3(b) shows a glass substrate after BOE etching using the proposed fabrication process. A very sharp geometry and a smooth etched surface are observed. Fig. 3(c) provides a schematic illustration of the experimental setup established to test the proposed circular micromixer. In this arrangement, a high-precision syringe pump (KDS-200, KD Scientific, USA) was used to generate the hydrodynamic driving forces. The two liquid samples chosen for mixing were DI water and a solution containing blue dye, respectively. The experimental tests were performed under a fluorescence microscope (E-400, Nikon, Japan). A CCD module (DXC-190, Sony, Japan) with a high-speed image acquisition interface (DVD PKB, V-gear, Taiwan) was used to acquire the optical images. The captured images were then analyzed using digital image techniques to evaluate the mixing performance.

Computational simulations

In general, comprehensive computational fluid dynamics simulations are conducted before physical models are built and tested since these simulations enable the system parameters to be varied over a wide range of values and permit the simultaneous and instantaneous data collection of various aspects of the model. Numerical simulation plays a key role in optimizing micromixer designs and enables a reliable interpretation of the experimental results.

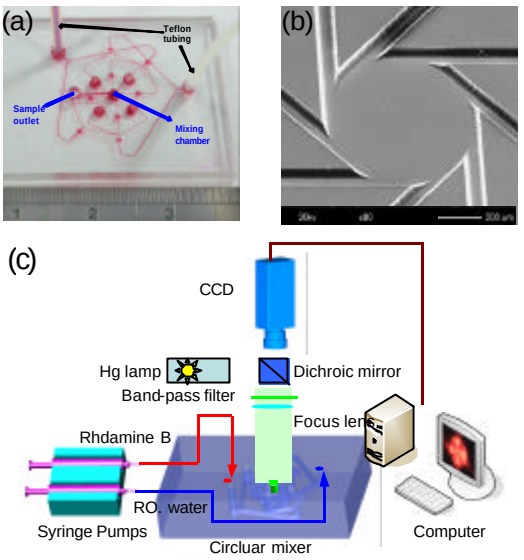

Figure 3: (a) Photographic image of micromixer following assembly. Note that channels are filled with red dye to enhance observation. (b) SEM image of close-up view for mixing chamber. (c) Schematic illustration of experimental setup.

The flow-field of a micro-mixer is governed by the incompressible Navier-Stokes equations. The governing conservation equations of mass, momentum and species are written respectively as:

$$\nabla_i u_i = 0 , \quad (1)$$

$$r\frac{\partial u_i}{\partial t} + r(u_j \cdot \nabla_j)u_i = -\nabla_i p + m\nabla^2 u_i , \quad (2)$$

$$\frac{\partial C}{\partial t} + (u_i \cdot \nabla_i)C = D\nabla^2 C , \quad (3)$$

where u_i denotes the fluid velocity, r the density, m the viscosity, D the binary diffusion coefficient, p the pressure, and C the concentration. In this calculation, the values of r, m and D are $1000 kg/m^3$, $0.001 kg/m/sec$ and $10^{-7} m^2/sec$ respectively.

As shown in Figure 1, the circular microchamber contains eight inlet microchannels and one outlet microchannel. In the present simulations, the inlet velocity of the eight inlets is set in the range 0.87 ~ 30 cm/sec, corresponding to Reynolds numbers of 0.5 ~ 17.1. In this study, the Reynolds number is defined as:

$$\mathrm{Re} = \frac{r u D_h}{m} \quad (4)$$

where D_h is the hydraulic diameter of the inlet microchannels. The fully developed condition is applied in the outlet microchannel. Meanwhile, the boundary condition of the microchamber wall is specified as a no-slip condition with a zero flux of the sample concentration. In order to provide good resolution, the computational domain is discretized with structure hexahedral meshes, with majority of the cells having

ISSN: 1727-1983

sides of 5 μm length. Hence, the current computational domain contains approximately 800,000 cells.

Results and discussion

Irrotational flow. The present numerical simulation results provide a very clear understanding of the physical phenomena which take place in the 3-dimensional vortex micromixer. Furthermore, the analytical results yield an accurate estimation of the mixing performance. Figure 4 presents the 3-dimensional streamline distributions in the circular microchamber at a Reynolds number of Re = 0.5. It can be seen that a 3-dimensional vortex does not exist under these flow conditions. On the other hand, flows with "sufficiently large" Reynolds number (the ratio of the inertia forces to the viscous forces) generally result in self-rotation of the fluid in the circular microchamber. However, flows in which the inertia forces are "small" compared with the viscous forces are characteristically laminar flows (irrotational flows). When Re = 0.5, the inertia forces in the circular microchamber are smaller than the viscous forces. Therefore, the 3-dimensional vortex is not formed and the streamlines simply flow directly from the inlet to the outlet. Figure 5 presents the cross-section streamline distributions at different heights in the circular microchamber when Re = 0.5. It is clear that a vortex is not induced at any cross-section. Although the streamlines are concentrated in a specific region at lower cross-sections (as shown in Figs. 5(a) and 5(b)), a vortex is not present. Note that the concentrated points mean the corresponding fluid outlet at their cross-sections.

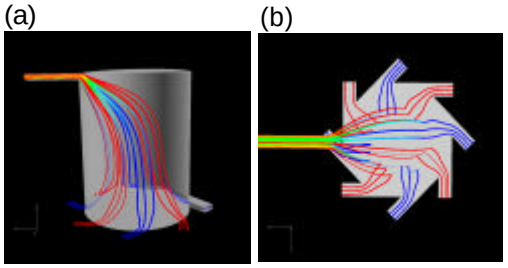

Figure 4: 3-dimensional streamline distributions in circular microchamber at Re=0.5: (a) side view and (b) top view.

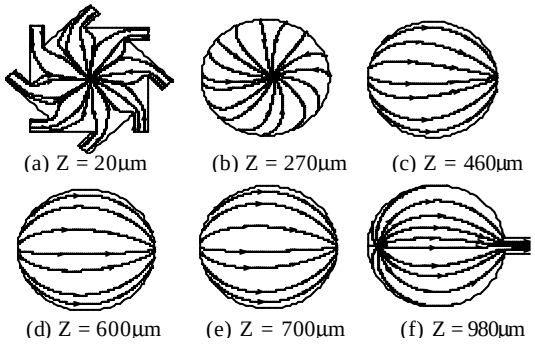

Figure 5: Cross-section streamline distributions at different heights in circular microchamber at Re=0.5: (a) Z = 20 μm, (b) Z = 270 μm, (c) Z = 460 μm, (d) Z = 600 μm, (e) Z = 700 μm, and (f) Z = 980 μm.

Figure 6 shows the numerical simulation results for the species concentration distributions at different cross-sections in the circular microchamber when Re = 0.5. As discussed above, a 3-dimensional vortex is not induced in the circular microchamber at this particular value of the Reynolds number. Therefore, at low Reynolds numbers, species mixing is dominated by diffusion of the two samples. From Figs. 6(a)-6(e), it is clear that the species concentration distribution has eight very distinct areas. In other words, a low Reynolds number flow fails to provide an effective species mixing. Figure 7 presents the species concentration contours at a cross-section located 100 μm downstream from the outlet and plots the normalized concentration intensity at three different heights for the cases of Re = 0.5 and Re =1.0. In this figure, the normalized concentration values of the two samples are 1 and 0, respectively. Consequently, a value of 0.5 indicates that the two samples are fully mixed. The normalized concentration profiles indicate that the mixing is far from complete at the three cross sections considered in this figure. To quantify the degree of mixing within the outlet channel, the present study adopts the following mixing efficiency parameter [7]:

$$s = \left(1 - \frac{\int_A |C - C_\infty| \, dA}{\int_A |C_0 - C_\infty| \, dA}\right) \times 100\% \qquad (5)$$

where C is the species concentration profile across the width of the mixing channel, and C_0 and C_∞ are the species concentrations in the completely unmixed (0 or 1) and completely mixed states (0.5), respectively. From the numerical results of Figs. 7(a) and 7(b), it can be shown that Reynolds numbers of 0.5 and 1.0 yield mixing efficiencies of 51.32% and 55.26%, respectively. This result confirms that irrotational flow fields in the circular microchamber yield a poor mixing performance within the mixing outlet.

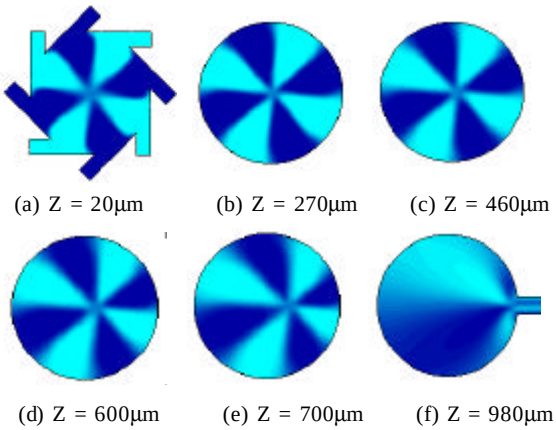

Figure 6: Numerical simulation results for species concentration distributions at different cross-sections in circular microchamber at Re=0.5: (a) Z = 20 μm, (b) Z = 270 μm, (c) Z = 460 μm, (d) Z = 600 μm, (e) Z = 700 μm, and (f) Z = 980 μm.

ISSN: 1727-1983

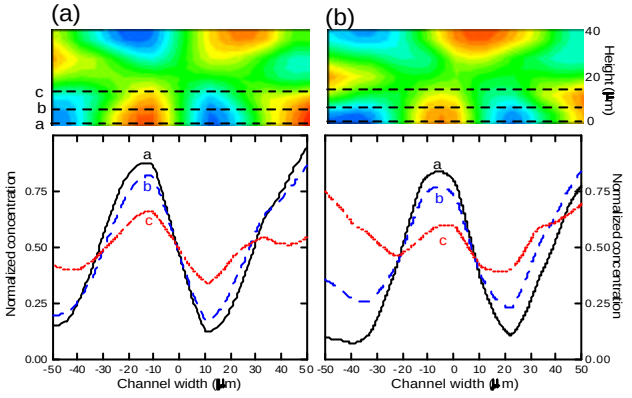

Figure 7: Species concentration contours at cross-section located 100 μm downstream from outlet and normalized concentration intensity at different heights at: (a) Re = 0.5 and (b) Re =1.0.

Self-Rotation Flow. In the microfluidic mixer, the mixing efficiency can be enhanced by increasing the contact area and the contact time of the different samples (i.e. by diffusive effects only), creating irregular flow fields (e.g. separation vortexes, coercive effects) in the mixing chamber, or by generating perturbations (coercive effects) of the sample fluids, etc. Of these various techniques, using irregular flow fields to enhance the mixing efficiency tends to be the most effective method. Accordingly, the present study utilizes self-rotation effects to induce a 3-dimensional vortex in the circular microchamber at low Reynolds numbers (*Re*) in order to enhance the mixing performance. The critical value of the Reynolds number, i.e. the value of the Reynolds number which marks the boundary between irrotational and rotational flow in the current circular microchamber, is 2.32. Therefore, an acceptable mixing performance can be obtained by establishing flows with Reynolds numbers of greater than 2.32.

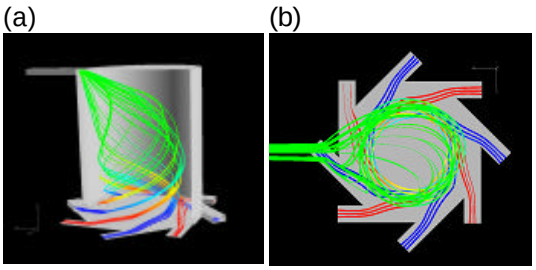

Figure 8: 3-dimensional streamline distributions in circular microchamber at Re = 3.2 (a) side view and (b) top view

Figure 8 presents the 3-dimensional streamline distributions in the circular microchamber at Re = 3.2. As this Reynolds number, the streamlines clearly indicate the self-rotation phenomenon and the presence of an induced 3-dimensional vortex. Figure 9 shows the cross-section streamline distributions at different heights in the circular microchamber when Re = 3.2. When the inertia forces are "sufficiently larger" than the viscous forces, self-rotation is induced in the circular microchamber. From Figure 9, it is obvious that a vortex exists at all cross sections other than the outlet cross section (Fig. 9(f)).

Figure 10 shows the numerical simulation results for the species concentration distributions at different cross-sections in the circular microchamber when Re = 3.2. When the samples are initially injected into the circular microchamber, the species concentration distribution has eight very distinct regions. The driving force is then applied to establish running sample flows with Reynolds number of 3.2. Consequently, self-rotation is induced in the circular microchamber and 3-dimensional vortex flows occur as a result. The spiral pattern resulting from the rotational flow field can be seen clearly in Figure 10. Figure 11 compares the species concentration contours at a cross-section located 100 μm downstream from the outlet for Re=3 and Re=6 and plots the corresponding normalized concentration intensities at different heights. The results show that the profiles of the normalized concentration intensity are very close to 0.5 (full mixing) throughout the circular chamber when Re = 6. The mixing efficiencies at the outlet region shown in Figs. 11(a) and 11(b) are determined to be 84.15% and 93.02%, respectively. Comparing Figure 11 with Figure 7, it can be seen that the self-rotation flows generated by the 3-dimensional vortex enhance the species mixing considerably.

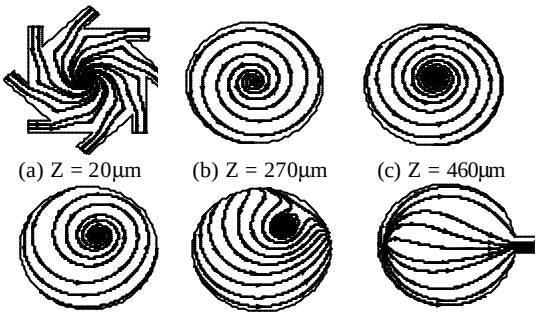

Figure 9: Cross-section streamline distributions at different heights in circular microchamber at Re=3.2: (a) Z = 20 μm, (b) Z = 270 μm, (c) Z = 460 μm, (d) Z = 600 μm, (e) Z = 700 μm, and (f) Z = 980 μm.

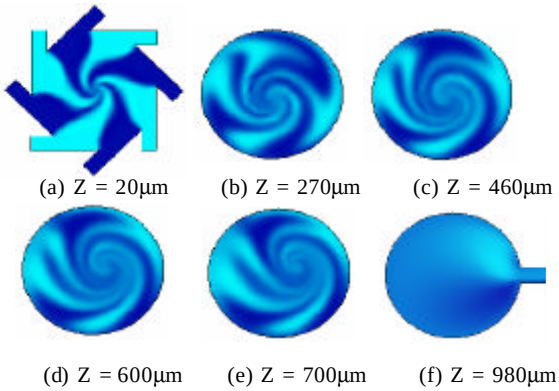

Figure 10: Numerical simulation results for species concentration distributions at different cross-sections in circular microchamber at Re=3.2: (a) Z = 20 μm, (b) Z = 270 μm, (c) Z = 460 μm, (d) Z = 600 μm, (e) Z = 700 μm, and (f) Z = 980 μm.

ISSN: 1727-1983

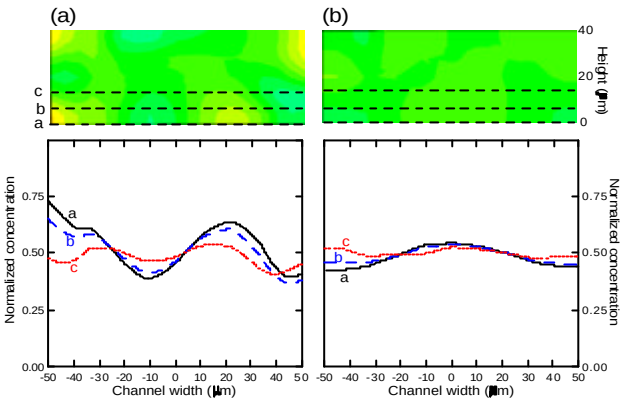

Figure 11: Species concentration contours at cross-section located 100 μm downstream from outlet and normalized concentration intensity at different heights at: (a) Re = 3 and (b) Re = 6.

Figure 12 presents the experimental flow images of the self-rotation in the circular microchamber mixer when Re = 3.2. Although in this figure, it is not possible to detect precisely the flow field conditions at any particular height within the microchamber mixer, a 3-dimensional vortex is clearly visible. More importantly, the experimental results are in good agreement with those achieved numerically. The optimized operating conditions for the current 3-dimensional vortex micromixer under different Reynolds numbers are presented in Figure 13. The optimal mixing efficiency is found to be greater than 90% for all the current tested cases. Hence, the feasibility of the proposed 3-dimensional vortex micromixer is confirmed.

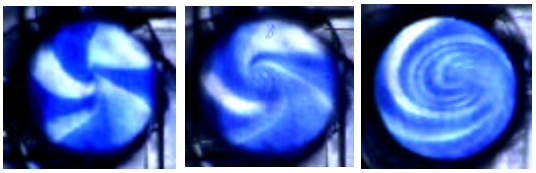

(a) Z ≈ 20 μm (b) Z ≈ 300μm (c) Z ≈800 μm

Figure 12: Experimental flow images of self-rotation in the circular microchamber mixer when Re = 3.2.

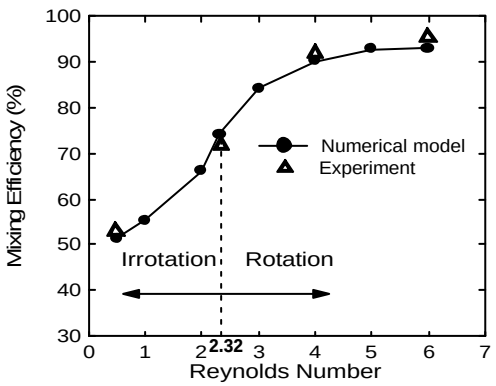

Figure 13: Numerical and experimental evaluations of mixing efficiency at different Reynolds number.

Conclusion

This study has developed a 3-dimensional vortex passive micromixer utilizing self-rotation in a circular microchamber. The microfluidic mixer is fabricated in a three-layer glass structure utilizing a simple and reliable fabrication process. A numerical model has been used to analyze the streamline distributions of the 3-dimensional vortex and to predict the mixing performance of the micromixer. The numerical results have indicated that when the Reynolds number is higher than a critical value of 2.32, a self-rotation effect is induced in the circular microchamber, which generates a 3-dimensional vortex. The mixing efficiency obtained in irrotational flow is less than 74% at a position of 100 μm downstream from the outlet microchannel. This performance may be insufficient to meet the requirements of certain applications. However, when self-rotation flow is established, the mixing efficiency can be increased to 90% when Re = 4. The numerical results are found to be consistent with the experimental results. The results presented in this study provide a valuable reference for the further development of integrated microfluidic chips with enhanced performance.

Acknowledgment

The current authors gratefully acknowledge the financial support provided to this study by the National Science Council of Taiwan under Grant Nos. NSC 93-2320-B-110-006 and NSC 93-2320-B-020-001.

References

[1] Ashton R., Padala C. and Kane R., (2003): 'Microfluidic separation of DNA', *Current Opinion Biotechnology*, 14, pp. 479-504

[2] Fiechtner G. J. and Cummings E. B., (2003): 'Faceted design of channels for low-dispersion electrokinetic flows in microfluidic systems' *Analytical Chemistry*, 75, pp. 4747-4755

[3] Kruger J., Singh K., O'Nel A., Jackson C., Morrison A. and O'Brien P., (2002): 'Development of a microfluidic device for fluorescence activated cell sorting', *Journal of Micromechanics and Microengineering*, 12, pp. 486-494

[4] Dodge A., Jullien M. C., Lee Y. K., Niu X., Okkels F. and Tabeling P., (2004): 'An example of a chaotic micromixer: the cross-channel micromixer', *Comptes Rendus Physique*, 5, 559-563

[5] Lemoff A. V. and Lee A. P., (2000): 'An AC magnetohydrodynamic micropump', *Sensors and Actuators B*, 63, pp. 178-185

[6] Oddy M. H., Santiago J. G. and Mikkelsen J. C., (2001): 'Electrokinetic instability micromixing', *Analytical Chemistry*, 73, pp. 5822-5832

[7] Lin C. H., Fu L. M. and Chien Y. S., (2004): 'Microfluidic T-form mixer utilizing switching electroosmotic flow', *Analytical Chemistry*, 76,pp. 5265-5272

[8] Niu X. and Lee Y. K., (2003): 'Efficient

ISSN: 1727-1983

spatial-temporal chaotic mixing in microchannels', *Journal of Micromechanics and Microengineering*, 13, pp. 454-462

[9] Yang R., Williams J. D. and Wang. W., (2004): 'A rapid micro-mixer/reactor based on arrays of spatially impinging micro-jets', *Journal of Micromechanics and Microengineering*, 14, pp. 1345-1351

[10] Yang Z, Goto H, Matsumoto M. and Maeda R, (2000): 'Active micromixer for microfluidic systems using lead-zirconate-titanate(PZT) -generated ultrasonic vibration', *Electrophoresis*, 21, pp. 116-119

[11] Bessoth F. G., deMello A. J. and Manz A., (1999): 'Microstructure for efficient continuous flow mixing', *Anal. Commun.*, 36, pp. 213-215

[12] Liu R. H., Stremler M. A., Sharp K. V., Olsen M. G., Santiago J. G., Adrian R. J., Aref H. and Beebe D. J., (2000): 'Passive mixing in a three-dimensional serpentine microchannel', *Journal of Microelectromechanical System*, 9, pp. 190-197

[13] Johnson T. J., Ross D. and Locascio L. E., (2002): 'Rapid Microfluidic Mixing', *Analytical Chemistry*, 74, pp. 45-51

[14] Stroock A. D., Dertinger S. K. W., Ajdari A., Mezic I., Stone H. A. and Whitesides G M., (2002): 'Chaotic mixer for microchannels', *Science*, 295, pp. 647-651

[15] Burke B. J. and Regnier F. E., (2003): 'Stopped-flow enzyme assays on a chip using a microfabricated mixer', *Analytical Chemistry*, 75, pp. 1786-1791.

[16] Chung Y. C., Hsu Y. L., Jen C. P., Lu M. C. and Lin Y. C., (2004): 'Design of passive mixers utilizing microfluidic self-circulation in the mixing chamber', *Lab on a Chip*, 4, pp. 70-77

[17] Kim D. S., Lee I. H., Kwon T. H. and Cho D. W., (2004): 'A barrier embedded Kenics micromixer', *Journal of Micromechanics and Microengineering*, 14, pp. 1294-1301

[18] Fu L. M. and Lin C. H., (2003): 'Numerical analysis and experimental estimation of a low leakage injection technique for capillary electrophoresis', *Analytical Chemistry*, 75, pp.5790-5796

ISSN: 1727-1983